LAWRENCE
LIVERMORE
NATIONAL
LABORATORY

LLNL-TR-410110

Characterization of Defocused Electron Beams and Welds in Stainless Steel and Refractory Metals using the Enhanced Modified Faraday Cup Diagnostic

J. W. Elmer

January 26, 2009

Disclaimer

This work performed under the auspices of the U.S. Department of Energy by Lawrence Livermore National Laboratory under Contract DE-AC52-07NA27344.

Characterization of Defocused Electron Beams and Welds in Stainless Steel and Refractory Metals using the Enhanced Modified Faraday Cup Diagnostic

By: John W. Elmer

January 23, 2009

Summary

As the first part of a project to compare new generation, continuous wave, laser welding technology to traditional electron beam welding technology, electron beam welds were made on commercially pure vanadium refractory metal and 21-6-9 austenitic stainless steel. The electron beam welds were made while employing EB diagnostics to fully characterize the beams so that direct comparisons could be made between electron beam and laser beams and the welds that each process produces.

Background and Introduction

Electron beam (EB) welding is a process that uses highly focused electrons accelerated to high energies to produce intense beams for welding. The process is performed in vacuum and produces very high quality precise welds with narrow heat affected zones [1]. EB welding has been used for the past 50 years to join high value added components in the aerospace and nuclear industries and has also found many other wide ranging applications. In comparison, high power lasers used for welding are relatively new, where 400W pulsed NdYAG welders were commercially available only since the early 1980's, and high power continuous wave lasers since the 1990's. Significant differences exist between lasers and electron beams used for welding, in that electron beam welding machines typically have very large focal lengths, use magnetic rather than conventional optics, and are performed in vacuum. One of the largest uncertainties in electron beam welding is the ability to control and repeat the focus of the beam due to imperfect magnetic optics and the wide variability of manufacturer specifications. Because of this, EB diagnostics have been explored [2-7], but have never achieved wide commercial acceptance. The previous work, combined with published work at LLNL [8-17] and patents at LLNL [18-26] has made significant progress in developing EB diagnostics that are reliable, repeatable, and employable in production environments.

Without the use of diagnostic tools the 'sharp focus' condition defined by an EB weld operator is subjective and, because of this, there is little known about the power distributions of electron beams used in the past. In this study, EB diagnostics will be used to characterize typical electron beam welds that are made in a defocused condition, which is often used to broaden out the fusion zone and ensure that the joint is covered. The EB diagnostic information is used to quantify the properties of these defocused beams, which is critical if these beams are to be produced on other EB welding machines. In addition to characterizing the beams, EB welds were made with fully characterized beams in vanadium and 21-6-9 stainless steel coupons, and characterized to determine the weld geometry and the surface roughness. This comparison demonstrates the effects of beam power distribution on vanadium, a refractory metal, where deep (keyhole) weld formation is difficult, and a 21-6-9 stainless steel where keyholes form more easily. The EB welds studied here are part of a larger investigation to evaluate the ability of modern continuous wave laser beams to duplicate electron beam welds. The laser welds are planned as future work, and will be performed using a laser beam focus monitor manufactured by Primes (www.primes.de) so that a one-to-one comparison can be made between electron beam and laser beam welding.

Experimental Procedure

Electron Beam Welding

Electron beam welds were made in vanadium and 21-6-9 stainless steel using a Hamilton Standard EB welder, serial number 605, fitted with a ribbon filament and an R-40 gun. A photograph of the welder is shown in Fig. 1 with its vacuum chamber door open. The

chamber size is approximately $1m^3$, and is typical of the types of electron beam welders used throughout industry for making relatively small electron beam welds in vacuum.

This EB machine was used to weld flat coupon samples of both materials in both bead-on-plate and step-joint configurations. The overall coupon dimensions are listed in Table 1, along with the LLNL drawing numbers for these parts. For the coupons with step joints, the step depth was approximately 50% of the coupon thickness. Two welds were made on each 6 inch long coupon, with each weld measuring approximately 2.5 inches long. After welding, metllographic samples were taken from the middle of each weld to examine the weld cross section geometry. These samples were prepared by conventional metallographic polishing and etching and were examined using optical light microscopy.

The welds were made by clamping the coupons into an aluminum hold down fixture which was placed 7 inch below the heat shield of the vacuum chamber. The weld joint was positioned such that it was running left-to-right as viewed by the operator. The EB diagnostic (see next section) was located in the chamber so that the top of the tungsten disk was at the same height as the top of the weld coupon. A separate tungsten target and a sacrificial stainless steel plate were also located at the same level as the top of the coupon. The purpose of the secondary tungsten target is to allow the operator to focus the beam as he normally would if diagnostics weren't being used, and the sacrificial stainless steel plate was scribed with parallel lines with a 25.4 mm spacing to set the circle diameter for the EB diagnostic. Once everything was set up, the EB chamber was pumped down to 10^{-6} torr, and then the pressure was increases to $1.8x10^{-4}$ torr just prior to performing the diagnostic measurements and making the welds.

The parameters used to make the EB welds are summarized in Table 2. The accelerating voltages used were either 110 kV (21-6-9) or 120 kV(vanadium), which are typical values for high voltage electron beam welders. The welds used relatively low beam currents, 5.5 mA (21-6-9) and 7.0 mA (vanadium), and moved at either 60 ipm (21-6-9) or 30 ipm (vanadium). In both cases the welds were defocused, which is commonly used to widen the weld to ensure that the weld joint was covered. Two different defocus settings were used in both materials to show the effects of a small defocus range, which might be required when trying to make the same weld on different EB welding machines. The different defocus values resulted in 2 different weld conditions for each material and joint geometry, resulting in 4 welds on each material. Electron beam diagnostic measurements were made during the same pump-down cycle as the welds, and were made before and after each weld to characterize the beams.

Electron Beam Diagnostics

The LLNL Enhanced Modified Faraday Cup (EMFC) diagnostic was used to measure the power density distribution of the electron beams [11, 12]. A photograph of the EMFC device is shown in Fig. 2, and the operating conditions can be found in [11]. This is the same diagnostic unit that is currently being used at LANL, Y-12, SNLL and KCP, and was designed for welds of 2kW total power or less such as the welds performed in this investigation. The EMFC device contains 17 linear slits placed at radial angles around a

tungsten slit disk. When the beam is deflected along a circular path of 25.4 mm in diameter, it passes over each slit, and a portion of the beam current is captured. The signal is then converted into a voltage drop across a known resistor and captured by a fast sampling analog-to-digital (A/D) converter before being transferred to the data acquisition software [17]. As the beam passes through each slit, it is sampled at a different angle, providing 17 different profiles of the beam shape after each revolution of the beam around the tungsten slit disk. The 17 waveforms represent the raw data and are collected by the data acquisition system as the beam passes over the tungsten slit disk. Figure 3a illustrates a series of these profiles for a sharp focused beam. If necessary, a digital filtering routine is applied to the data to remove any electronic noise which may appear. Note that all of the data taken in this study was very clean from electronic noise, and no filtering was required or used for all of the data that is presented here. The data are then fed into a computer assisted tomographic (CT) imaging algorithm in order to reconstruct the power density distribution of the beam [17]. All of the data was reconstructed with the default settings of the LLNL CT software with a profile length of 490 and a resize factor of 2. The resize factor of 2 reduces the number of data points so the resulting data can be directly read into other spreadsheets and plotting programs for post-processing, such as the 3-D rendition of the power density distribution presented in Fig. 3b.

Once the beam has been CT reconstructed, the peak power density of the electron beam and two distribution parameters are then measured as indicated in Fig. 3c. The first distribution parameter is the full width of the beam at one-half its peak power density (FWHM), which represents the width at 50% of the beam's peak power density. The second parameter is the full width of the beam measured at $1/e^2$ of its peak power density (FWe2), which represents the width of the beam at 86.5% of the beam's peak power density. FWe2 is often considered to be a suitable representation of the beam diameter. Since the cross section of the measured beam is not always circular, the area of the beam at these two points is measured, and the diameter of a circle having the same area is used to represent both values. These approximations are good for most beams with generally circular cross sectional shapes, such as the Gaussian-like distributions typically found near the sharp focus setting, however, for defocused beams, the circular approximation may not be as accurate.

A total of 16 beams were examined using the EMFC and version 2.1 of the LLNL CT software. These diagnostic runs represent the before and after conditions of the electron beams for each of the eight welds. A typical screen shot from one of the defocused beams (+45 defocus) used to make a vanadium weld at 120kV, 7.0mA, is presented in Fig 4a, showing all the data used for the reconstruction along with the beam parameters. This same beam is shown in a 3-D surface plot format in Fig 4b. Note the differences of approximately 10x in the peak power density of this beam compared with the sharp focused 120kV, 7.0mA, beam shown previously in Fig 3b. Similar data are presented for one of the defocused beams used to make one of the 21-6-9 welds in Fig. 5 (+45 defocus). Note the kidney shape of these beams, which is caused by an astigmatism of the electron beam optics combined with the fact that the beam is defocused [16]. Also note that the long side of the beam (major axis) is oriented perpendicular to the direction of weld

travel which effectively broadens the beam. The aspect ratio of the beam is calculated by the CT software program and is presented in the lower right hand corner of the printout screens in Figures 4 and 5, showing that the beam's major axis is rotated approximately 80º from horizontal, and has an aspect ratio of approximately 1.6:1 (1.36mm/0.85mm).

Materials

Commercially pure vanadium plate was obtained in 3 mm thick sheets from existing LLNL stock on hand. This material is nearly pure vanadium but contains 0.0340%Si, 0.0052%C, 0.0004% H, 0.0170% N, and 0.0100% O, in wt%. The 21-6-9 stainless steel, also know as Nitronic 40, was obtained in 6 mm thick plae from known weldable 21-6-9 stainless steel on hand at LLNL. This material is a nitrogen-strengthened austenitic stainless steel and contains 19.96%Cr, 9.14%Mn, 7.02 %Ni, 0.23%N, 0.04%Al, 0.02%C, 0.05%Si, 0.014%P, <0.005%S, <0.001%O, bal Fe in wt%. This stainless steel is commonly referred to as 21-6-9 based on the nominal amounts of chromium, nickel, and manganese, respectively, present in the alloy. The high manganese content of the Nitronic 40, which is over four times higher than in the 304 stainless steel (9.14 vs. 1.71%) and the high nitrogen content, which is nearly three times higher (0.23 vs. 0.082%), result in a material that keyholes during EB welding much easier than conventional stainless steels and vanadium due to the high vapor pressure of manganese and the volatility of nitrogen [27].

The welding coupons were prepared from both materials by conventional machining, followed by lapping to produce a 1.6μm RMS finish on the top surface of the coupons. These samples were solvent cleaned prior to assembling in the weld fixture for welding.

Results and Discussion

EB Diagnostics

The EMFC was used to not only measure the properties of the electron beams before and after each weld, but to also first determine the sharp focused condition for each of the welding parameters. This first step is critical in providing a point of reference for the welds which will be made in a defocused condition.

In order to determine the sharp focus condition, the operator first set the beam parameters (kV and mA) and then focused the beam on the tungsten target, just as one would do if no EB diagnostics were present. This starting condition, known as the operator's sharp focus, can sometimes be off by as much as 5mA or more, even with experienced welding operators. Once the operator's sharp focus is established, the EMFC was used to measure its beam parameters. Next, the focus coil current was incremented in 5mA steps to intentionally defocus the beam from the starting condition, and the EMFC was used to measure this beam. This process was repeated for both positive and negative deviations from the operator's sharp focus setting until a clear minimum was established in the

beam's FWHM and FWe2, and a corresponding clear maximum was established in the peak power density of the beam. These data are plotted up and the focus setting corresponding to the minimum beam size and corresponding peak power density was determined. This value is the true sharp focus condition and all other focus settings are referenced to it.

Table 3 summarizes the EMFC data for the beams used to find sharp focus and to make the bead-on-plate welds. For the 110kV, 5.0mA beam, the sharp focus condition was determined to be at a focus coil current of 761mA. This beam had a peak power density (PPD) of 14.2kW/mm^2, a FWHM value of 0.188mm and a FWe2 value of 0.316mm. At 120 kV, 7.0mA, the sharp focus condition was determined to be at a focus coil current of 801mA. This beam had a higher peak power density (PPD) of 19.9kW/mm^2, but a similar FWHM of 0.188mm and FWe2 0.315mm. Using these respective sharp focus values, the welds were made at defocus values of +40 to +50mA, as indicated in Table 3. In both cases the PPD of the defocused beams dropped by more than 10x while the FWHM and FWe2 values increased by more than 3x as compared to the sharp focus condition.

The EB diagnostic results for the bead-on-plate welds from Table 3 are plotted in Figure 6, which shows the PPD, FWHM and FWe2 as a function of defocus relative to the sharp focus condition. All of the data is plotted in the left most three figures, which show the PPD, FWHM and FWe2 near the location of the sharp focus and for the defocused beams. The maximum in the PPD and the minimum in the FWHM and FWe2 are located at the relative focus setting of zero. The defocused beam measurements made just before and after the welds, are shown in the three rightmost figures. These figures zoom in on the defocused beam data for better resolution. The before and after weld diagnostic results show variations of 5% or less, which is typical for these measurements [8].

Table 4 summarizes the EMFC data for the beams used to find sharp focus and make the step-joint welds. These welds were made approximately 1 month after the bead-on-plate welds, so the diagnostic data is a good measure of how repeatable the electron beam welder is over a 1 month period of time. For the 110kV, 5.0mA beam, the sharp focus condition was determined to be at a focus coil current of 760mA, which is nearly identical to the value determined previously. This beam had a peak power density (PPD) of 14.9kW/mm^2, a FWHM value of 0.194mm and a FWe2 value of 0.312mm. All three values are within 5% of the previous measurements. At 120 kV, 7.0mA, the sharp focus condition was determined to be at a focus coil current of 798mA which is again close to the previously determined value. This beam had a peak power density (PPD) of 19.9kW/mm^2, a FWHM of 0.190mm and FWe2 0.318mm, which are all again within 5% of the previously determined values. Using these respective sharp focus values, the welds were made at defocus values of +40 to +50mA, as indicated in Table 4. As before, the PPD of the defocused beams dropped by more than 10x while the FWHM and FWe2 values increased by more than 3x as compared to the sharp focus condition.

The EB diagnostic results from Table 4 for the step-joint welds are plotted in Figure 7, which shows the PPD, FWHM and FWe2 as a function of defocus relative to the sharp

focus condition. All of the data is plotted in the left most three figures, which show the PPD, FWHM and FWe2 near the location of the sharp focus and for the defocused beams. The maximum in the PPD and the minimum in the FWHM and FWe2 are located at the relative focus setting of zero. The defocused beam measurements made just before and after the welds are shown in the three rightmost figures. In the case of the step joint welds, there was more variation of the peak power density before and after the weld than with the step-joint welds, but the FWHM and FWe2 had similar variations as before.

Electron Beam Welds

The EB diagnostic information that was collected before and after each of the welds is summarized in Table 5 for convenience, which gives the peak power density, FWHM and FWe2 for each of the 16 beams. The FWHM varied between 0.59 and 0.82mm with peak power densities on the order of 1kW/mm^2 to 1.5kW/mm^2 for the different conditions used to make the welds. The relatively large diameter of the beams and the correspondingly low peak power densities are the result of the large amount of defocus used to generate these beams. Sharp focused beams of the same parameters have an order of magnitude higher power densities indicated in Figures 6 and 7, and would have significantly higher penetration depths than those of the defocused beams.

Weld cross sections and some weld longitudinal sections were prepared from the welded samples to determine the depth and width of the 8 welds, and the results are summarized in Table 6, indicating weld penetrations on the order of 1mm. Figure 8 shows the bead-on-plate welds in vanadium for the two defocus conditions. Since vanadium grows large grains in the heat affected zone, it can be difficult to determine the fusion boundary, and it takes careful observation under a microscope to determine the weld depth and width. Fig. 8a shows the weld that had the larger amount of defocus (+50) was measured to be 0.89 mm and its width to be 2.20 mm. In comparison, the weld made at the smaller amount of defocus (+45) had deeper penetration of 1.04 mm and approximately the same width of 2.30 mm. Thus the higher power density of the less defocused beam of 1442W/mm^2 produced approximately 17% increase in penetration over the more defocused beam with a peak power density of 1141W/mm^2. The 17% increase in penetration is less than the 26% increase in the peak power density. The longitudinal sections are shown in Fig. 8, indicating the deeper penetration of the less defocused beam that had the higher power density.

The 21-6-9 bead-on-plate welds are shown in Fig. 9. for the two defocus conditions. Figure 9a shows the weld that had the larger amount of defocus (+45). The depth of this weld was measured to be 0.60mm and its width to be 1.52mm. The weld made with the lower amount of defocus (+40) had deeper penetration of 0.76mm but approximately the same width as the other weld of 1.47mm. Again, the higher power density weld had the deeper penetration, where the depth of penetration increased 26% (0.60 to 0.76mm) as the power density increased 26% (1027 vs 1303 W/mm^2). The longitudinal sections through the welds are also shown in Fig. 9. These micrographs show a clear transition between the fusion zone and the base metal, and indicate the uniformity of penetration at the weld root.

The step-joint welds were made with the same EB parameters as the bead-on-plate welds and all show deeper penetration than the bead on plate welds. Figure 10 shows the cross sections of the vanadium step-joint welds for a) the +45 defocus and b) the +50 defocus. The penetration increases from 1.12mm to 1.20mm as the defocus decreases and the power density increases. The 7% increase in penetration is less than for the bead-on-plate welds under the same condition where the peak power density increased by 14% for these conditions. Figure 11 shows the cross sections of the 21-6-9 step-joint welds for a) the +40 defocus and b) the +50 defocus. The penetration increases from 0.96mm to 1.05mm as the defocus decreases and the power density increases. This represents a 9.4% increase in penetration, which again is less than that of the bead-on-plate welds under similar percentage increases in the peak power density.

A comparison of the bead-on-plate welds with the step-joint welds shows that the bead-on-plate welds all had lower penetrations than the step-joint welds by a significant amount. The reason for this is related to the presence of the joint, which can allow a gap to be present for easier transport of electrons below the surface, and/or the different heat flow conditions where the bottom side of the step which can act as a heat transfer barrier and allow the heat to concentrate more below the weld. The other difference between the two joint designs, is that, for the range of parameters investigated, the bead-on-plate welds showed increases in penetration that were similar to increases in the peak power density of the beam, whereas for the step-joint welds the penetration increase was much less.

Surface Roughness

The cross sectional views of the welds show that they are raised up in the center and that there is some undercutting that seems to favor one side of the weld. In order to quantify this topology, the surface roughness was measured on the bead-on-plate welds using a profilometer. The results of the vanadium welds are presented in Fig. 12, which shows the profile across the top surface of the weld at approximately its midpoint. The profile for the vanadium weld with the +50 defocus is shown in Fig 12a, and indicates that the depression caused by the undercut is 30μm, and the hump in the center is 80μm. This gives a 110μm total distance between the lowest and highest points. The profile for the vanadium weld with the +45 defocus is shown in Fig. 12b, showing a larger undercut of 60μm and a hump of 73μm, for a total variation of 133μm. In both cases, the samples were reasonably flat, except for the local variations caused by the weld fusion zone.

The results of the 21-6-9 stainless steel welds are presented in Figure 13, which also gives the surface profile across the weld bead near its midpoint. The profile for the 21-6-9 weld with the +45 defocus is shown in Fig 13a, indicating that the undercut is 31μm below the original surface, and the hump is 60μm above the original surface, resulting in a total variation of 91μm. The profile for the 21-6-9 weld with the +40 defocus was nearly identical, showing an undercut of 28μm, and a hump of 61μm, for a total variation of 89μm. In both 21-6-9 welds, the surface was not nearly as flat as the vanadium welds, where there is an angular distortion that hinged the plates upward about the centerline of

the weld. The resulting distortion caused approximately 0.25mm distortion over 10mm width of the plate, which corresponds to an angle of 1.4 deg.

A comparison of the surface profiles for the two materials shows that there was slightly more peak to valley difference in the vanadium welds than in the 21-6-9 stainless steel. This is most likely due to the fact that the weld heat input per unit length was higher for the vanadium welds than for the 21-6-9 welds. For the four welds, the average undercut measured 39μm below the original surface, and the average hump above the original surface measured 69μm. The largest difference between the two materials was the amount of distortion that occurred in the plates, where the vanadium showed almost zero angular distortion, the 21-6-9 showed 1.4 deg of angular distortion. The reason for the difference is most likely due to the material properties, where the strength of the 21-6-9 is considerably higher than that of the vanadium, allowing higher residual stresses to be generated during welding.

Conclusions

1. Electron beam diagnostics were used to characterize the properties of defocused beams produced by a high voltage electron beam welder operating in the 110kV to 120kV range at 5.5 to 7.0 mA.
2. Defocusing the electron beams by +40 to +50 mA, resulted in a decrease in the peak power density of the beams by approximately 10X, and caused a corresponding increase in the beam width (FWHM) and beam diameter (FWe2) of approximately 3X as compared to the corresponding sharp focused beams.
3. Repeated beam measurements made one month apart showed that the beams reproduced themselves within 5% of the peak power density, FWHM and FWe2.
4. Welds were made on vanadium and 21-6-9 stainless steel, in the both bead-on-plate and step-joint configurations using fully characterized defocused beams. The results showed that small changes in the defocus setting resulted in measurable changes in the beam properties and a corresponding change in the weld penetrations.
5. The weld penetrations varied from 0.6 to 1.2 mm, and all weld penetrations increased with increases in the peak power density of the beam. For the step-joint welds, the penetrations were all greater than those of the bead-on-plate welds, but they showed less variation in penetration with the peak power density.
6. Surface roughness was measured on the welds, indicating that there was an undercut on one side of the weld which averaged 39μm below the original surface, and there was a hump in the middle of the welds that averaged 69μm for the 4 welds measured.
7. The vanadium welds exhibited less angular distortion than the 21-6-9 welds. The vanadium surface was nearly flat after welding, while the 21-6-9 showed a 1.4 deg upward angular distortion.

Acknowledgement

This work performed under the auspices of the U.S. Department of Energy by Lawrence Livermore National Laboratory under Contract DE-AC52-07NA27344. This document was prepared as an account of work sponsored by an agency of the United States government. Neither the United States government nor Lawrence Livermore National Security, LLC, nor any of their employees makes any warranty, expressed or implied, or assumes any legal liability or responsibility for the accuracy, completeness, or usefulness of any information, apparatus, product, or process disclosed, or represents that its use would not infringe privately owned rights. Reference herein to any specific commercial product, process, or service by trade name, trademark, manufacturer, or otherwise does not necessarily constitute or imply its endorsement, recommendation, or favoring by the United States government or Lawrence Livermore National Security, LLC. The views and opinions of authors expressed herein do not necessarily state or reflect those of the United States government or Lawrence Livermore National Security, LLC, and shall not be used for advertising or product endorsement purposes. I would like to thank Mr. Mark Gauthier of LLNL for performing the electron beams welds, Mr. Jackson Go of LLNL for performing the optical metallography, and Mr. Alan Teruya for assisting with the electron beam diagnostic software.

References

1. Recommended Practices for Electron Beam Welding, 1992. *American Welding Society*, ANSI/AWS C7.1-92.

2. L. N. Tallerico and W. H. Giedt: *Welding Journal*, 1988, 67(12):299-s to 305-s.

3. G. K. Hicken, W. H. Giedt, and A. E. Bentley: *Welding Journal*, 1991, 70(3):69-s to 75-s.

4. Y. Arata: in 'Plasma, Electron and Laser Beam Technology', ASM International, 1986, pp. 3-27.

5. U. Dilthey and J. Weiser: *Schw. and Schn.*, 1995, 47(7): pp. 558-564.

6. U. Dilthey and J. Weiser: *Schw. and Schn.*, 1995, 47(5): pp. 339-345.

7. G. R. LaFlamme and D. E. Powers: *Welding Journal*, 1991, 70(10): pp. 33-40.

8. T.A. Palmer and J.W. Elmer, Improving Process Control in Electron Beam Welding Using the Enhanced Modified Faraday Cup, *Journal of Manufacturing Science and Engineering*, 130(4), 041008, 2008.

9. T. A. Palmer, J. W. Elmer, K. D. Nicklas, and T. Mustaleski, "Transferring Electron Beam Parameters Using the Enhanced Modified Faraday Cup," *Welding Journa*l,

86(12), pp 388s-398s, 2007.

10. T.A. Palmer and J.W. Elmer, "Characterization of Electron Beams at Different Focus Settings and Work Distances in Multiple Welders Using the Enhanced Modified Faraday Cup", *Science and Technology of Welding and Joining*, 12(2), pp 161-174, 2007.

11. J. W. Elmer, A. T. Teruya, and T. A. Palmer "User's Guide: An Enhanced Modified Faraday Cup for the Profiling of the Power Density Distribution in Electron Beams," *Lawrence Livermore National Laboratory*, UCRL-MA-148830, 59 pages, August, 2002.

12. J. W. Elmer and A. T. Teruya, "An Enhanced Faraday Cup for the Rapid Determination of the Power Density Distribution in Electron Beams," *Welding Journal*, 80 (12), pp 288s-295s, 2001.

13. J. W. Elmer, A. T. Teruya and P. E. Terrill, "Electron Beam Welding of a Depleted Uranium Alloy to Niobium Using a Calibrated Electron Beam Power Density Distribution," UCRL-ID-141043, October, 2000.

14. J. W. Elmer and A. T. Teruya, "Fast Method for Measuring Power-Density Distribution of Non-Circular and Irregular Electron Beams," *Science and Technology of Welding and Joining*, Vol 3, No. 2, p. 51, 1998.

15. J. W. Elmer, A. T. Teruya and M. Gauthier, "Beam Profile Analysis for the C&MS B231 Electron Beam Welding Machines," *Lawrence Livermore National Laboratory*, UCRL-ID-127549, June 12, 1997.

16. J. W. Elmer, A. T. Teruya and D. W. O'Brien, " Tomographic Imaging of Non-Circular and Irregular Electron Beam Power Density Distributions," *Welding Journal* 72 (11), p 493-s, 1993.

17. A. T. Teruya, J. W. Elmer and D. W. O'Brien, "A System for the Tomographic Determination of the Power Distribution in Electron Beams," *The Laser and Electron Beam in Welding, Cutting, and Surface Treatment State-of-the-Art 1991*, Bakish Materials Corporation, p 125, 1991.

18. Alan T. Teruya, John W. Elmer, Todd A. Palmer, and Chris C. Walton, "Miniature Modified Faraday Cup for Micro Electron Beams," U. S. Patent Number 7,378830, B2, issued May 27, 2008.

19. John W. Elmer, Alan T. Teruya, Todd A. Palmer, "Electron Beam Diagnostic for Profiling High Power Beams," U. S. Patent Number 7,348,568 B2, issued March 25, 2008.

20. John W. Elmer, Alan T. Teruya, Todd A. Palmer, Chris C. Walton, “Diagnostic System for Profiling Micro-Beams,” U.S. Patent No. 7,288,772, issued October 30, 2007.

21. John W. Elmer, Todd A. Palmer, Alan T. Teruya, “Trigger Probe for Determining the Orientation of the Power Distribution of an Electron Beam,” U. S. Patent Number 7,244,950 B2, issued July 17, 2007.

22. John W. Elmer and Alan T. Teruya, “An Enhanced Modified Faraday Cup for the Fast Determination of the Power Density Distribution in Non-Circular and Irregular Electron Beams,” U. S. Patent Number 6,300,755, issued October 9, 2001.

23. Alan T. Teruya and John W. Elmer, “Tomographic Determination of the Power Distribution in Electron Beams,” U. S. Patent Number 5,583,427, issued December 10, 1996.

24. John W. Elmer, Alan T. Teruya, Dennis W. O’Brien, “Modified Faraday Cup,” U. S. Patent Number 5,554,926, issued September 18, 1996.

25. John W. Elmer, Alan T. Teruya, Dennis W. O’Brien, “System for Tomographic Determination of the Power Density Distribution in Electron Beams,” U. S. Patent Number 5,468,966, issued November 21, 1995.

26. John W. Elmer, Alan T. Teruya, Dennis W. O’Brien, “A System for Tomographic Determination of the Power Density Distribution in Electron Beams,” U. S. Patent number 5,382,895, issued January 17, 1995.

27. T. A. Palmer, B. Wood, J. W. Elmer, C. Westrich, J. O. Milewski, M. Pilch, M. Barbe, and R. Carpenter, "Characterization of Stainless Steel and Refractory Metal Welds Made Using a Diode-Pumped, Continuous Wave Nd:YAG Laser," *Lawrence Livermore National Laboratory*, UCRL-ID-146005, 39 pages, November, 2001.

Table 1: List of vanadium and 21-6-9 stainless steel coupons for the electron beam welds, along with LLNL drawing numbers and overall dimensions

Drawing	Description	Dimensions L x W (mm)	Material
AAA08-501242-AC	Intermediate Plate Tab1	140x30	Vanadium
AAA08-501241-AC	Intermediate Female	140x15	Vanadium
AAA08-501240-AC	Intermediate Male	140x15	Vanadium
AAA08-501245-AB	Outer Plate Tab 1	150x30	21-6-9 SS
AAA08-501244-AA	Outer Male	150x25	21-6-9 SS
AAA08-501243-AA	Outer Female	150x25	21-6-9 SS

Table 2: Summary of electron beam welding. Bead-on-plate (BOP) welds and step-joint welds were made on 21-6-9 stainless steel and vanadium coupons. All welds were made in the defocused condition.

Weld	Material	Voltage (kV)	Current (mA)	Focus Setting (mA)	Relative Focus (mA)
BOP					
1	Vanadium	120	7.0	851	+50
2	Vanadium	120	7.0	846	+45
3	21-6-9	110	5.5	806	+45
4	21-6-9	110	5.5	801	+40
Step-Joint					
5	Vanadium	120	7.0	843	+45
6	Vanadium	120	7.0	848	+50
7	21-6-9	110	5.5	800	+40
8	21-6-9	110	5.5	805	+45

Table 3: Summary of the EB diagnostic data used for welding the flat coupons. Data for finding sharp focus and the measured properties of the defocused beams are listed. Diagnostic measurements indicated as –A were made right before a weld, and –B measurements were made immediately after the weld.

Voltage (kV)	Beam Current (mA)	Focus Setting (mA)	Relative Focus (mA)	PPD (W/mm^2)	FWHM (mm)	FWe2 (mm)
21-6-9 SS						
110	5.5	756	-5	12138	0.215	0.327
		761*	0	14186	0.188	0.316
		766	5	13296	0.188	0.327
		771	10	10657	0.209	0.361
		776	15	6425	0.254	0.461
		801-A**	40	1262	0.633	1.09
		801-B**	40	1250	0.639	1.094
		806-A**	45	968	0.724	1.247
		806-B**	45	992	0.718	1.239
Vanadium						
120	7.0	796	-5	19530	0.196	0.306
		801*	0	19895	0.188	0.315
		806	5	16826	0.196	0.343
		811	10	12414	0.237	0.39
		846-A**	45	1401	0.719	1.197
		846-B**	45	1479	0.698	1.168
		851-A**	50	1152	0.801	1.329
		851-B**	50	1133	0.815	1.333

* Sharp focus setting as determined by the EMFC

** Defocused beams measured before and after the flat coupon welds

Table 4: Summary of the EB diagnostic data used for welding the step-joint coupons. Data for finding sharp focus and the measured properties of the defocused beams are listed. Diagnostic measurements indicated as –A were made right before a weld, and –B measurements were made immediately after the weld.

Voltage (kV)	Beam Current (mA)	Focus Setting (mA)	Relative Focus (mA)	PPD (W/mm^2)	FWHM (mm)	FWe2 (mm)
21-6-9 SS						
110	5.5	750	-10	5607	0.346	0.464
		755	-5	12542	0.22	0.376
		760*	0	14874	0.194	0.312
		765	5	14559	0.191	0.324
		770	10	12545	0.205	0.345
		775	15	8995	0.23	0.403
		780	20	6091	0.272	0.479
		800-A**	40	1310	0.6	1.06
		800-B**	40	1390	0.59	1.04
		805-A**	45	1050	0.66	1.19
		805-B**	45	1100	0.64	1.15
Vanadium						
120	7.0	786	-12	6832	0.368	0.489
		791	-7	14449	0.243	0.433
		796	-2	19491	0.198	0.319
		801	3	19516	0.192	0.323
		798*	0	19914	0.19	0.318
		806	8	17711	0.194	0.341
		811	13	14025	0.224	0.38
		816	18	9358	0.27	0.461
		821	23	6160	0.324	0.567
		843-A**	45	1410	0.68	1.19
		843-B**	45	1480	0.66	1.15
		848-A**	50	1180	0.75	1.31
		848-B**	50	1100	0.77	1.36

* Sharp focus setting as determined by the EMFC

** Defocused beams measured before and after the step-joint welds

Table 5: Summary of the 16 electron beam diagnostic measurements made before (A) and after (B) each of the welds, grouped into like focus conditions. The average, standard deviation, and the ratio of the standard deviation to the average value are highlighted for each of the four EB weld parameter groupings.

Material	Joint	Focus Setting (mA)	Relative Focus (mA)	Power Density (W/mm^2)	FWHM (mm)	FWe2 (mm)
Vanadium	BOP	851-A	50	1152	0.8	1.33
Vanadium	BOP	851-B	50	1133	0.82	1.33
Vanadium	Step	848-A	50	1180	0.75	1.31
Vanadium	Step	848-B	50	1100	0.77	1.36
			avg	1141	0.79	1.33
			std	33.6	0.03	0.02
			std/avg (%)	2.9	3.96	1.55
Vanadium	BOP	846-A	45	1401	0.72	1.2
Vanadium	BOP	846-B	45	1479	0.7	1.17
Vanadium	Step	843-A	45	1410	0.68	1.19
Vanadium	Step	843-B	45	1480	0.66	1.15
			avg	1442	0.69	1.18
			std	42.9	0.03	0.02
			std/avg (%)	3.0	3.74	1.88
21-6-9	BOP	806-A	45	968	0.72	1.25
21-6-9	BOP	806-B	45	992	0.72	1.24
21-6-9	Step	805-A	45	1050	0.66	1.19
21-6-9	Step	805-B	45	1100	0.64	1.15
			avg	1027	0.69	1.21
			std	59.3	0.04	0.05
			std/avg (%)	5.8	6.02	3.85
21-6-9	BOP	801-A	40	1262	0.63	1.09
21-6-9	BOP	801-B	40	1250	0.64	1.09
21-6-9	Step	800-A	40	1310	0.6	1.06
21-6-9	Step	800-B	40	1390	0.59	1.04
			avg	1303	0.62	1.07
			std	63.5	0.02	0.02
			std/avg (%)	4.9	3.87	2.29

Table 6: Summary of the weld depths and weld widths for the 8 different welds.

Weld	Material	Relative Focus (mA)	Travel Speed (ipm)	Weld Depth (mm)	Weld Width (mm)	Depth to Width Ratio
BOP						
1	V	+50	30	0.89	2.20	0.40
2	V	+45	30	1.04	2.30	0.45
3	21-6-9	+45	60	0.60	1.52	0.39
4	21-6-9	+40	60	0.76	1.47	0.52
Step						
5	V	+45	30	1.20	2.31	0.52
6	V	+50	30	1.12	2.40	0.47
7	21-6-9	+40	60	1.05	1.51	0.70
8	21-6-9	+45	60	0.96	1.59	0.60

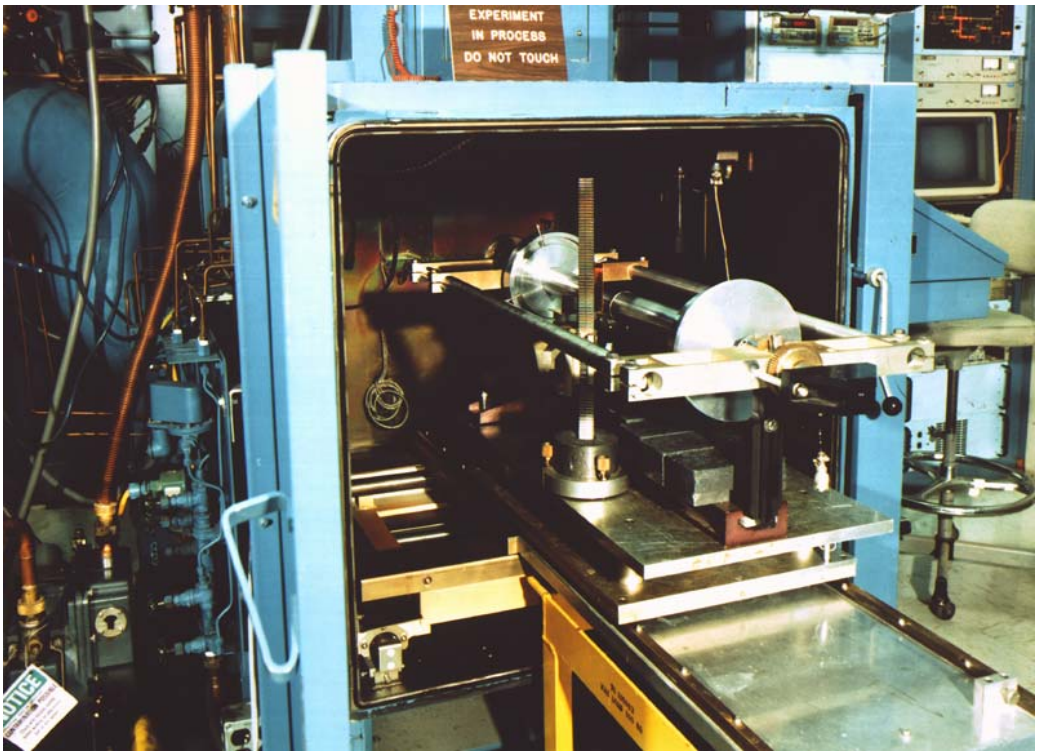

Figure 1: Hamilton Standard electron beam welder SN605 used in this study.

Figure 2. Photograph of the Enhanced Modified Faraday Cup. The diagnostic is approximately 100mm high, 75 mm in diameter and weighs approximately 1kg.

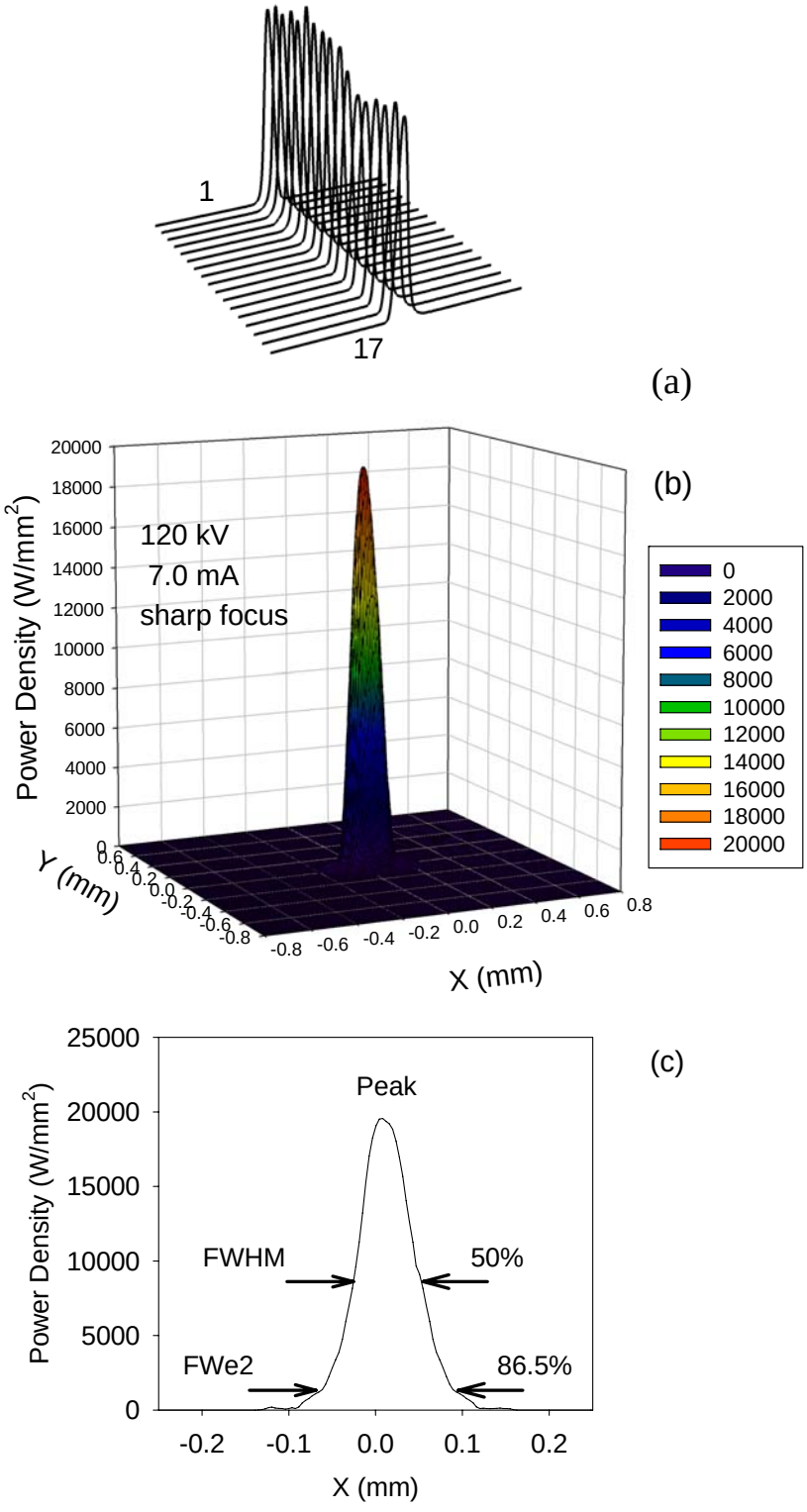

Figure 3: Overview the EMFC data for the 120kV, 7.0mA sharp focused beam. (a) A series of profiles seen by all 17 slits, (b) 3D tomographic reconstruction of the power density distribution, and (c) slice through the center of the reconstructed beam with the peak power density, FWHM, and FWe2 measurements indicated.

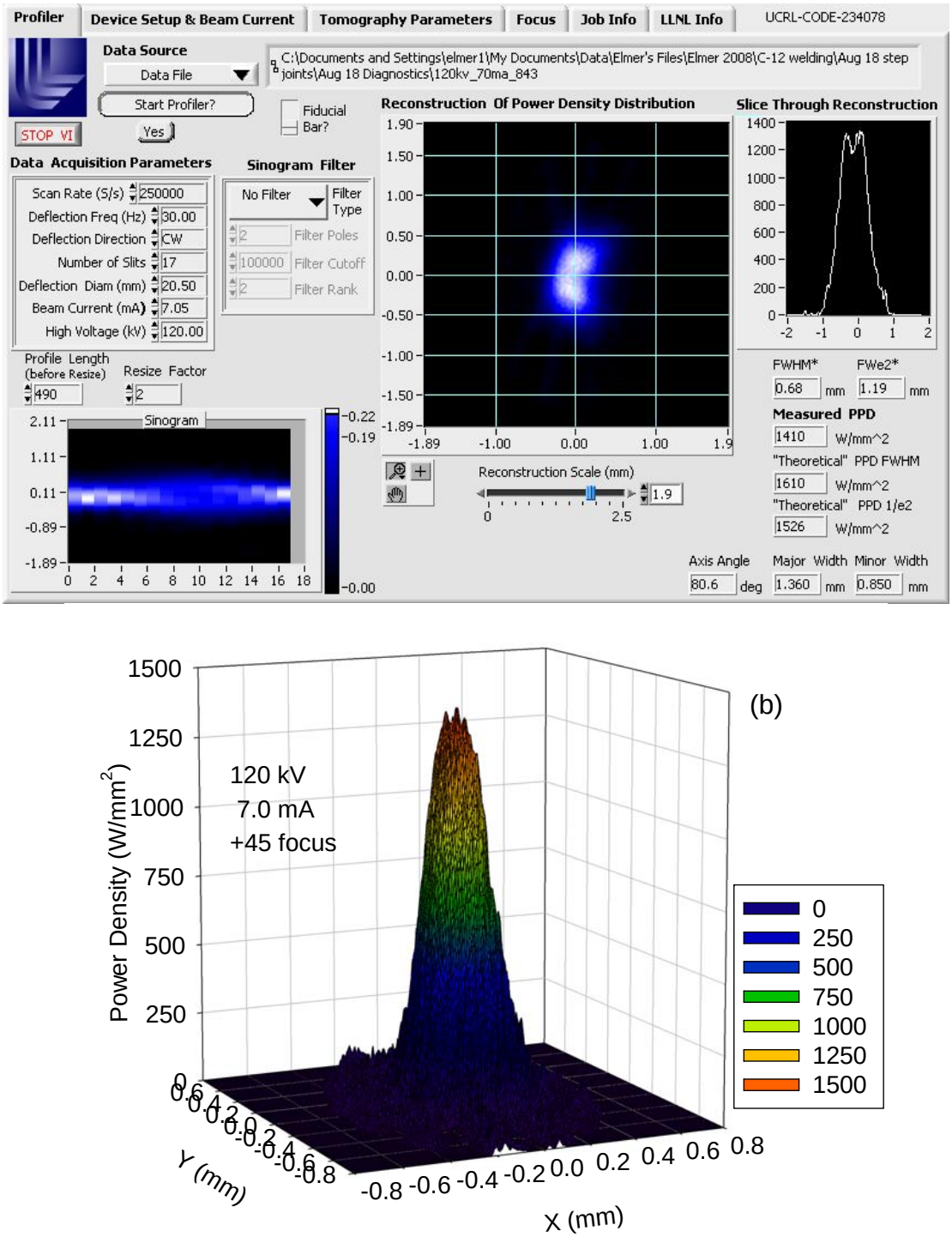

Figure 4: Reconstruction screen shot for a 120kV, 7.0mA defocused beam (+45) used to make one of the vanadium welds, and surface mesh plot of the reconstructed beam.

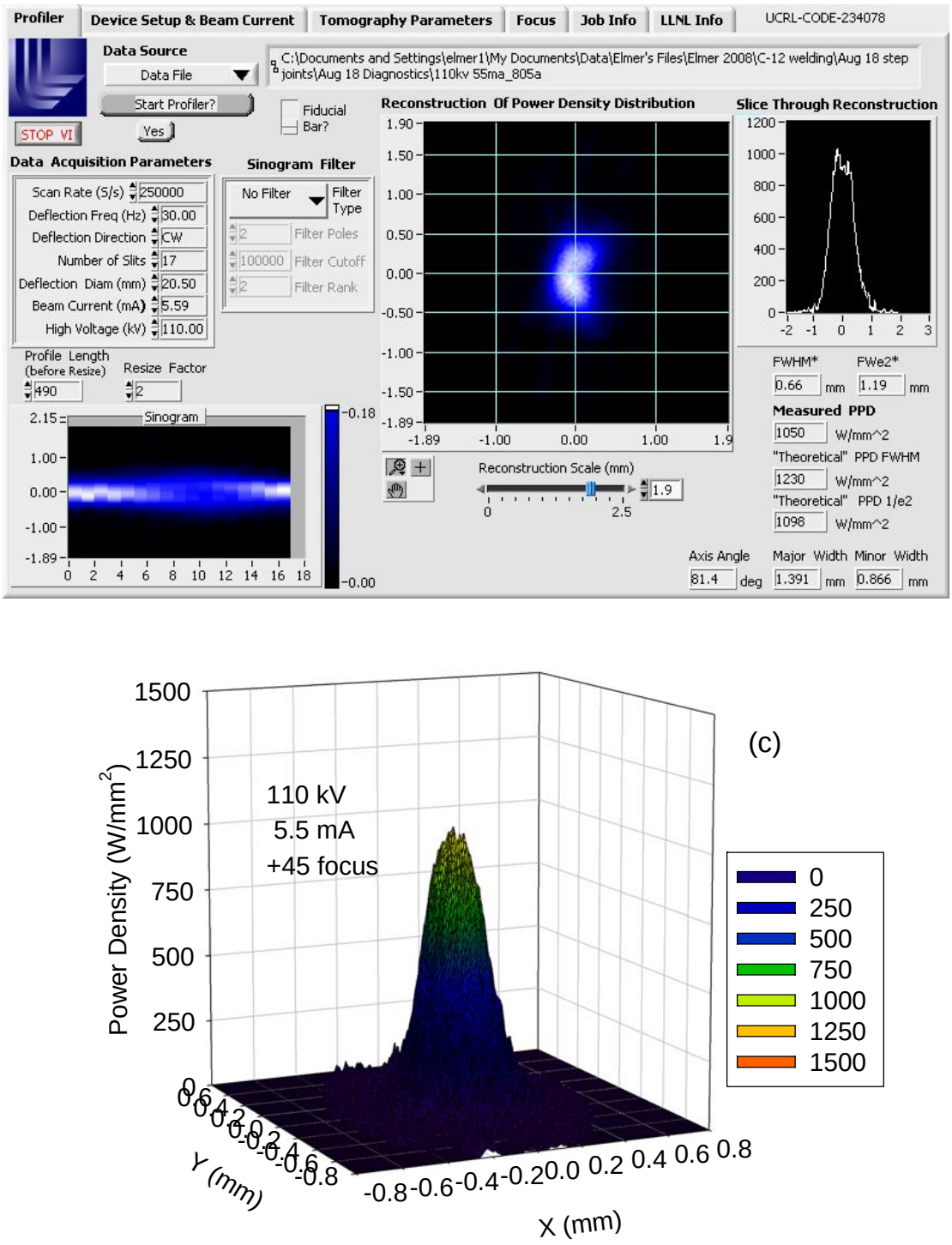

Figure 5: Reconstruction screen shot for a 110kV, 5.5mA defocused beam (+45) used to make one of the 21-6-9 steel welds, and surface mesh plot of the reconstructed beam.

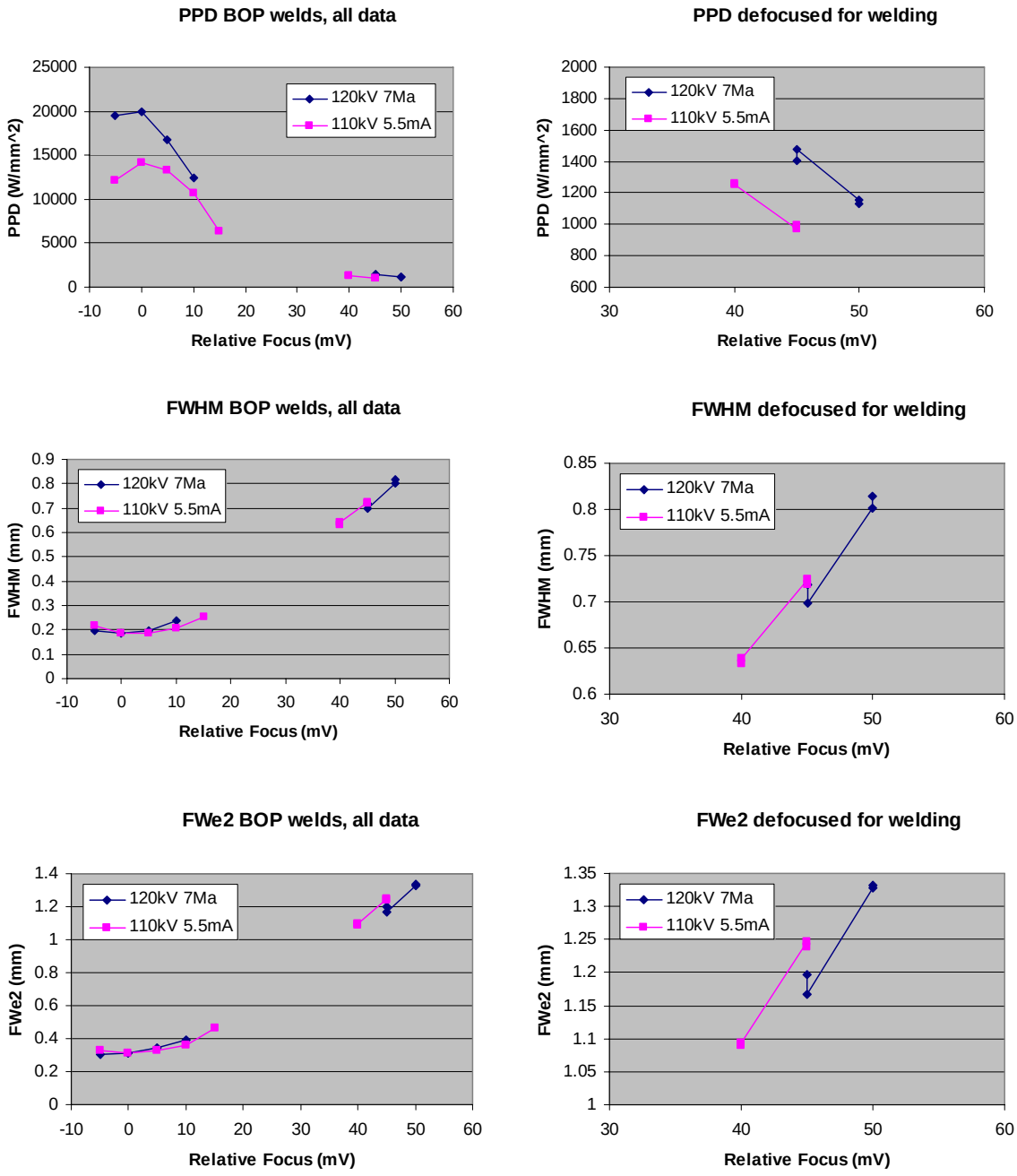

Figure 6: Diagnostic measurements of the electron beams used to make the bead-on-plate welds. The left column shows peak power density (PPD), full width at half maximum (FWHM) and full width at $1/e^2$ (FWe2) for all the data as a function of relative focus. Sharp focus is located at a relative focus value of zero. The rightmost figures zoom in on the PPD, FWHM, and FWe2 data showing the defocused conditions used to make the welds. Two data points were taken for each weld, one before and one after each weld completion.

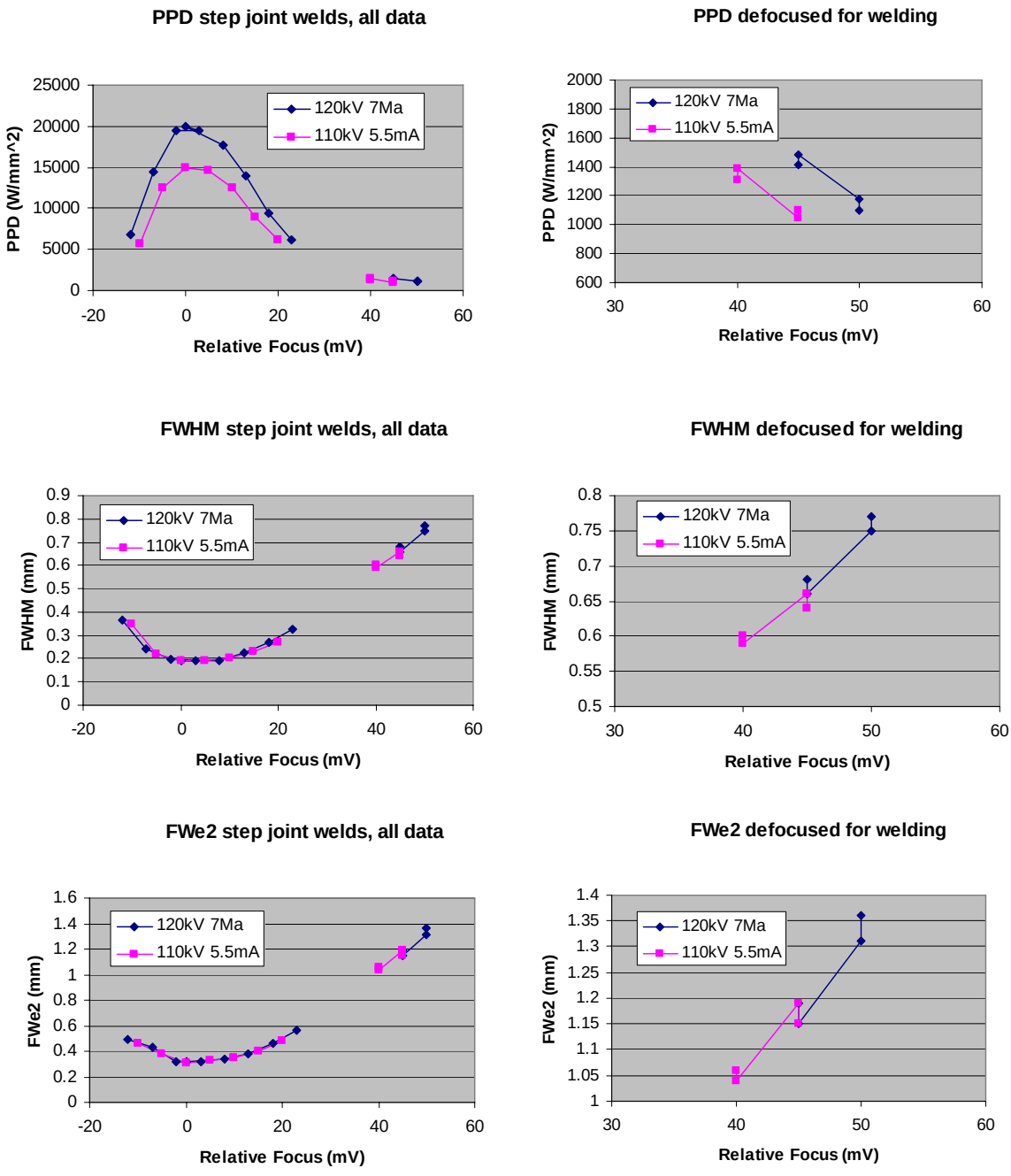

Figure 7: Diagnostic measurements of the electron beams used to make the step-joint welds. Similar to the data presented in Figure 6, where two data points were taken for each weld, one before and one after each weld completion.

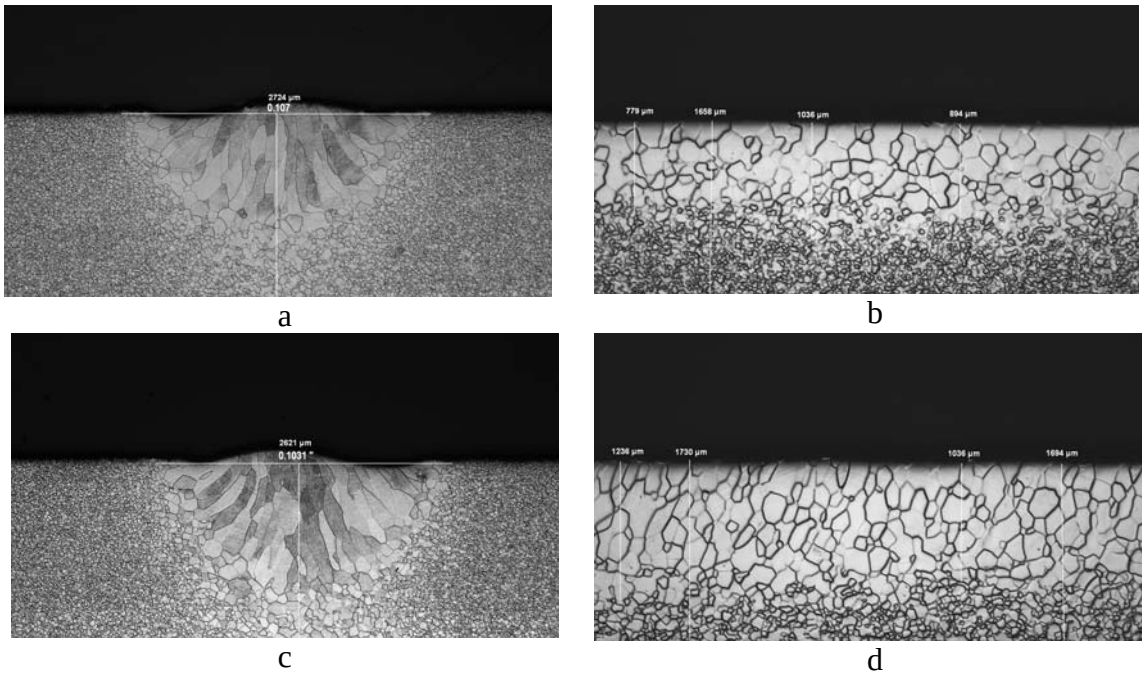

Figure 8: Results of the bead-on-plate electron beam welds on vanadium. a) Weld 1 cross section (+50 defocus), b) weld 1 longitudinal section, c) weld 2 cross section (+45 defocus), d) weld 2 longitudinal section.

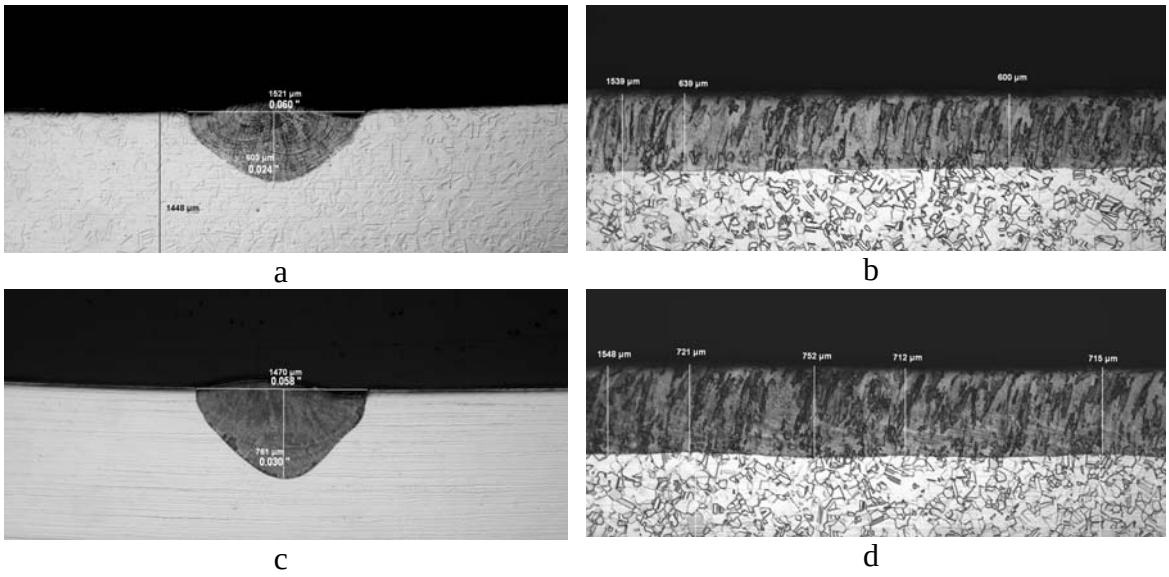

a b

c d

Figure 9: Results of the bead-on-plate electron beam welds on 21-6-9 stainless steel. a) Weld 3 cross section (+45 defocus), b) weld 3 longitudinal section, c) weld 4 cross section (+40 defocus), d) weld 4 longitudinal section.

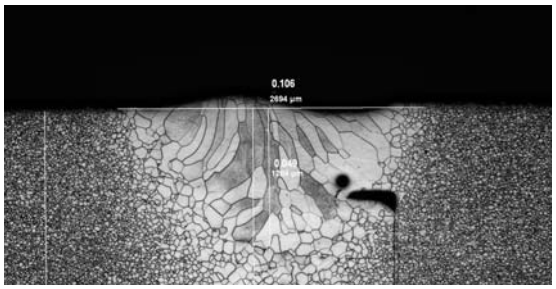

a

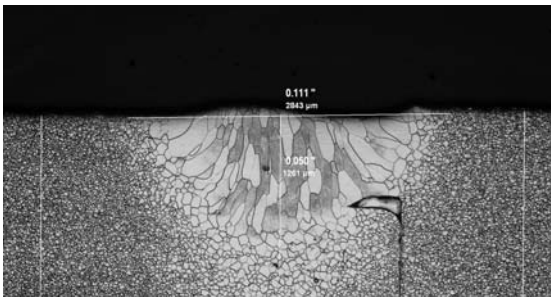

b

Figure 10: Results of the step-joint electron beam welds on vanadium. a) Weld 5 cross section (+45 defocus), b) weld 6 cross section (+50 defocus).

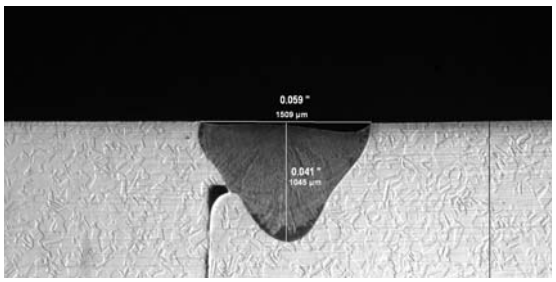

a

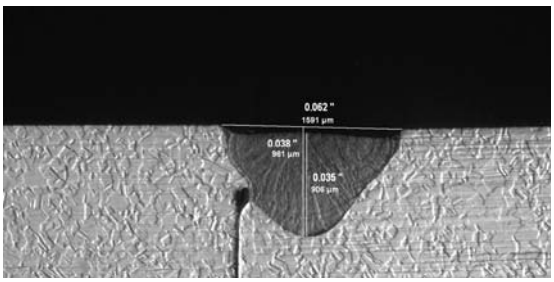

b

Figure 11: Results of the step-joint electron beam welds on 21-6-9 stainless steel. a) Weld 7 cross section (+40 defocus), b) weld 8 cross section (+45 defocus)

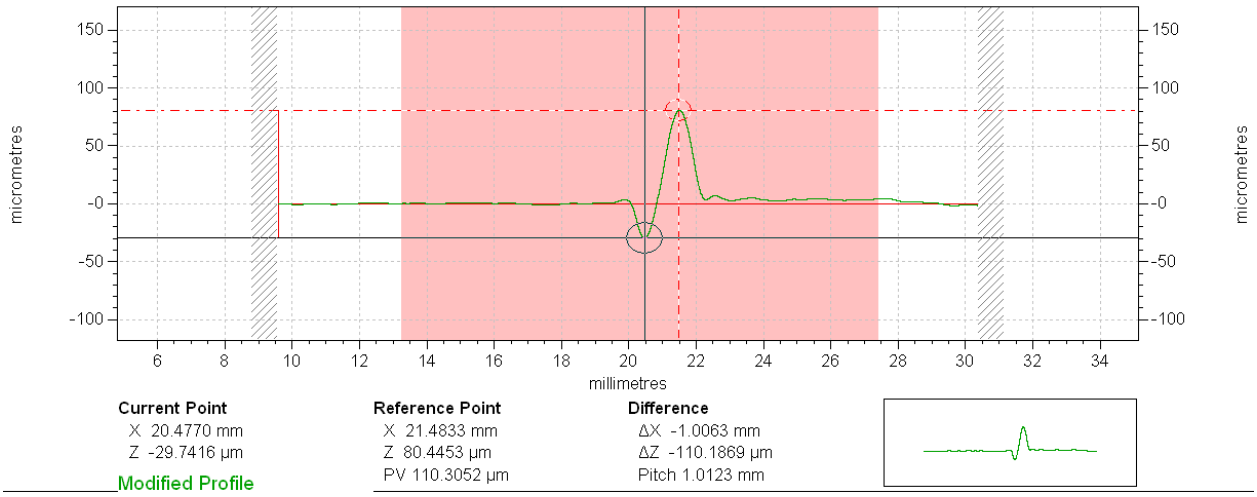

(a)-Weld 1

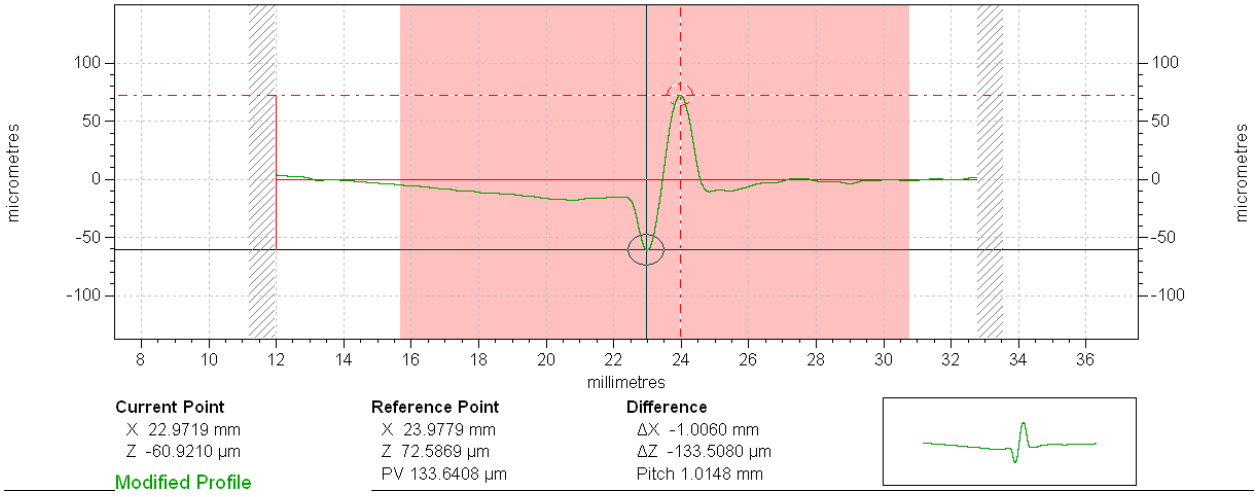

(b)- Weld 2

Figure 12: Surface profiles across the top surface of the vanadium bead-on-plate welds. a) 120kV, 7.0mA, 30ipm, +50 defocus, b) 120kV, 7.0mA, 30ipm, +45 defocus.

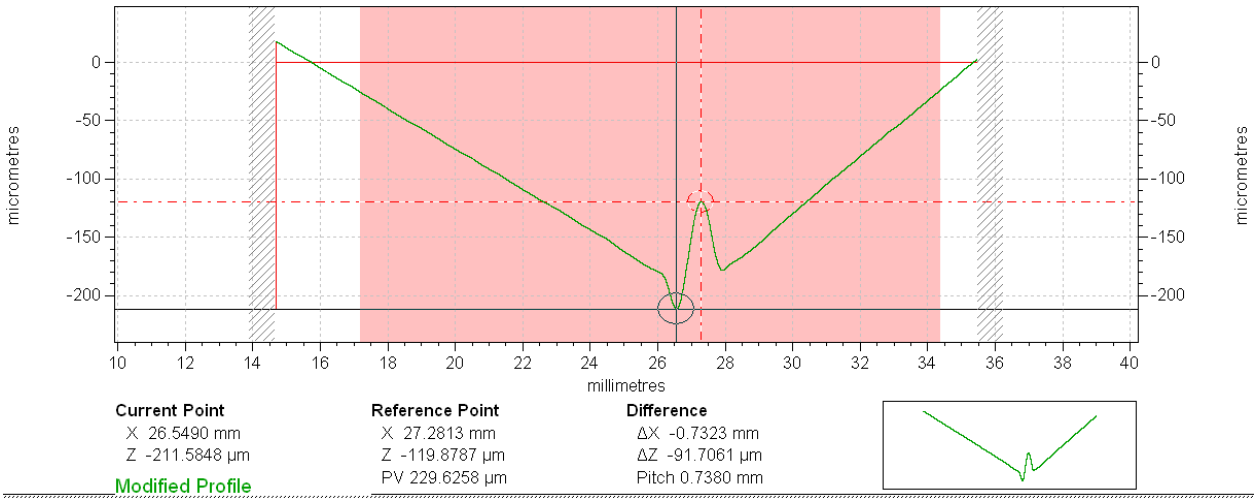

(a)-Weld 3

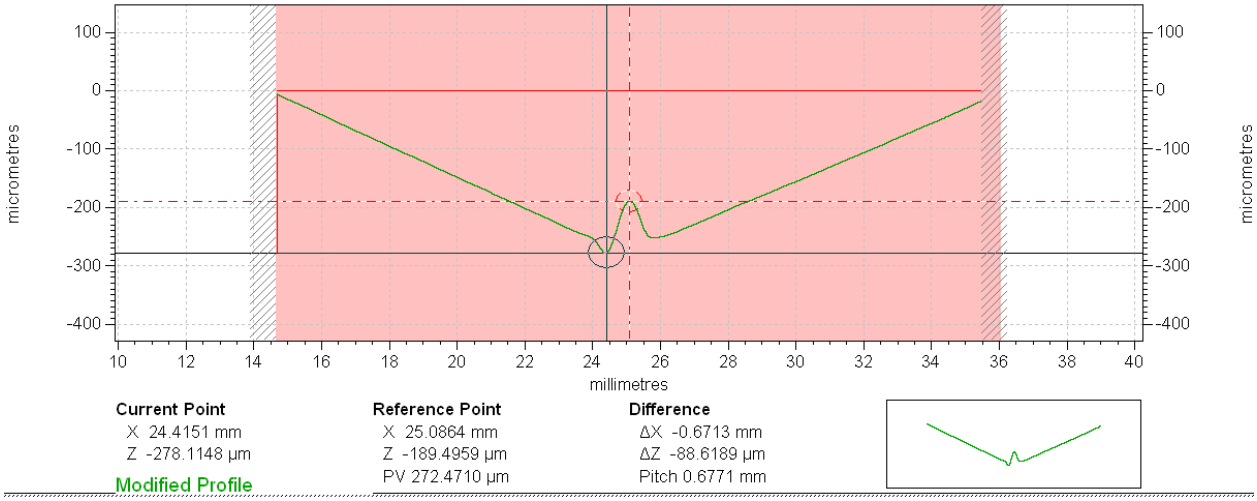

(b)- Weld 4

Figure 13: Surface profiles across the top surface of the 21-6-9 bead-on-plate welds. a) 110kV, 5.5mA, 60ipm, +45 defocus, b) 110kV, 5.5mA, 60ipm, +40 defocus.